# Minimizing Indoor Sound Energy with Tunable Metamaterial Surfaces

**2 authors:**

Sichao Qu
The University of Hong Kong
**12** PUBLICATIONS   **176** CITATIONS

SEE PROFILE

Ping Sheng
The Hong Kong University of Science and Technology
**563** PUBLICATIONS   **41,194** CITATIONS

SEE PROFILE

Some of the authors of this publication are also working on these related projects:

Room Acoustics with Metamaterials View project

Wave Functional Materials View project

# Minimizing Indoor Sound Energy with Tunable Metamaterial Surfaces

Sichao Qu[*] and Ping Sheng[†]

*Department of Physics, Hong Kong University of Science and Technology, Hong Kong 999077, China*

The advent of broadband and tunable acoustic metamaterials, amenable to be fabricated into flat panel geometry, offers broad, emerging possibilities for room acoustics. In particular, the fine tuning of surface acoustic impedance becomes possible to optimize specific room acoustic goals. In this initial simulation study we examine the possibility of minimizing the averaged level of energy density ($L_e$), both globally and locally in an enclosed room. The relationship curve between surface impedance and global $L_e$ shows an optimal value that can reduce $L_e$ by about 15–20 dB over a wide audible frequency regime. Moreover, partial coverage of the room surface by the optimally tuned acoustic metamaterial already demonstrates considerable effectiveness. We compare and verify our numerical model with the statistical-diffusive acoustics model and find good agreement in the high-frequency regime. In the low-frequency regime, the energy inhomogeneity caused by wave interference can be utilized to create a quiet zone for specific targeted frequency by optimally tuning the surface impedance values at discretized locations on the four walls.

## I. INTRODUCTION

Room acoustics is the science of using acoustic reflection, scattering [1], and absorption [2] to manipulate the indoor auditory experience [3,4]. With the exception of scattering, which is mostly controlled by geometric patterning of the walls and their tilt angles; reflection and absorption are functions of the complex impedance of the room surfaces, defined here to comprise the walls, ceiling, and the floor. If we discount acoustic transmission through the wall and ceiling, then reflection and absorption are related through energy conservation [5]; and impedance of the room surfaces offers an important handle in determining the room acoustics. In this context, the recent breakthrough in broadband tunable acoustic impedance via structural metamaterials [6–9] offers the latest possibilities for attaining various indoor acoustics objectives. In this work, we use model simulations with arbitrary boundary impedance to explore the potential in lowering the global $L_e$, as well as the local $L_e$ (i.e., a quiet zone in the presence of an indoor noise source). The results show that a maximum reduction of about 20–25 dB of global $L_e$ can be achieved, with partial coverage of room surfaces by optimized acoustic metamaterials also found to be fairly effective. Compared to the existing works that reduce $L_e$ by adopting sound sensors and actively controlled sources or panels [10–12] (involving complex algorithms to cancel the sound field), our work systematically studies the

general requirement on the impedance values of the room surfaces with broadband merits. In addition, by using a genetic algorithm [13] to optimize the discretized surface impedance values and their placement on the wall, the realization of a quiet zone is shown to be possible, by taking advantage of the low-frequency interference effect. It should be noted that actively tunable metasurface [14] has achieved a local quiet zone, or hotpot at a single frequency, by using a simple iterative optimization scheme [15]. However, the optimized region is limited to the vicinity of one spatial point, targeted in the high-frequency regime with reverberated sound field.

The outline of this paper is as follows. Section II presents the simulation setup and relevant definitions, while Sec. III provides a theoretical framework of impedance tunable metamaterials. Results for minimizing global $L_e$ are presented in Sec. IV, which includes the following. First, global $L_e$ variation is plotted as a function of the surface impedance, treated here as a real number ranging from nearly 0 to $10^3 Z_0$, where $Z_0$ denotes the air impedance. The numerical results are seen to agree well with the prediction of the statistical-acoustics model (based on the diffusive equation) [16–19] when the relevant wavelength is short compared to the characteristic room size. Second, it is shown that there is an optimal impedance value at which global $L_e$ attains a minimum, and the variation of this optimal impedance value with frequency is presented. Third, global $L_e$ spectra with hard boundary and optimal boundary impedance are compared. Also, the inclusion of the imaginary part of the impedance for the broadband acoustic metamaterials is shown to have

_____

[*]squ@connect.ust.hk
[†]sheng@ust.hk
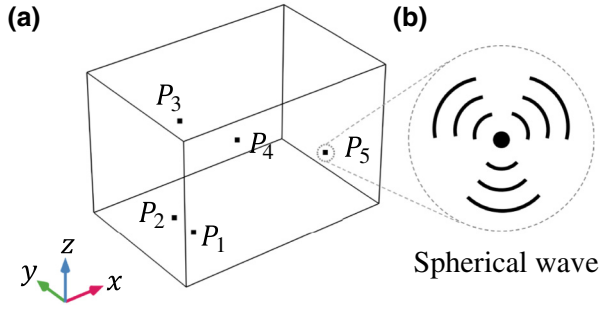
**(a)**

**(b)**



Spherical wave

FIG. 1. (a) Schematics of the enclosed room with five randomly placed sound sources. (b) Enlarged view of the sound source that emits spherical waves.

a negligible effect on the previous results. Fourth, the effectiveness of partial coverage of the room surfaces is examined. In Sec. V, surface impedances at discretized surface areas are assigned given values with the objective of minimizing the local $L_e$ at a given location. It is shown that it is possible to lower the local $L_e$ from an indoor noise source by optimal utilization of both wall absorption and wave interference effect. Section VI summarizes the main conclusions.

## II. MODEL DEFINITIONS

Our simulations are carried out with either a multiple number of sound sources, denoted multisource [see $P_1, P_2, P_3, P_4, P_5$ in Fig. 1(a)], or a single sound source, denoted monosource [see $P_1$ in Fig. 1(a)], within a room with the dimension of $2 \times 2 \times 3$ m³. These sources emit spherical waves [see Fig. 1(b)] with different power and phases, specified in Appendix A. Surface impedance of the room is tuned between $Z \to 0$ (soft boundary) and $Z = 10^3 Z_0$ (hard boundary), which is the impedance range of most common materials [20]. Sound energy density at a specific position is defined by the summation of kinetic and potential energy,

$$\epsilon = \frac{1}{2}\rho_0 v^2 + \frac{1}{2}\frac{1}{K_0}p^2. \quad (1)$$

Here $p$ and $v$ denote acoustic pressure and displacement velocity, respectively. For air, the density $\rho_0 = 1.2$ kg/m³ and adiabatic stiffness $K_0 = \rho_0 c_0^2 = \gamma P_0 = 1.41 \times 10^5$ Pa, where $c_0$ is airborne sound speed, with $P_0$ being the atmospheric pressure and $\gamma = 1.4$ being the adiabatic index of air.

The objective is to adjust the surface impedance and minimize the averaged sound level of energy density ($L_e$) [21], defined as

$$L_e = 10 \log_{10}\left(\frac{1}{V}\int_V \frac{\epsilon}{\epsilon_0}dV\right) = 10 \log_{10}\left(\frac{\bar{\epsilon}}{\epsilon_0}\right), \quad (2)$$

with $\epsilon_0 = 10^{-12}$ J/m³. Here $L_e$ can be converted to sound pressure level ($L_p$) (see Appendix B). The impedance associated with the minimum $L_e$ is defined to be "optimal." Accordingly, if $V$ denotes the volume of the whole room (or a selected volume in the room), then the minimization of the global $L_e$ (or local $L_e$) is the objective.

Wave phenomena are closely related to the ratio between the size of the object and the wavelength. Hence, we define a characteristic length of the room as $l_0 = \sqrt[3]{V}$ and its corresponding characteristic frequency is

$$f_0 = \frac{c_0}{l_0}. \quad (3)$$

In the present model, $f_0 \cong 150$ Hz serves as the unit frequency to present the results in the dimensionless way. If $f/f_0 < 1$, there is almost no eigenmodes for the soft boundary, i.e., $Z < Z_0$, as discussed in Appendix C that has the important consequence of suppressing the sound source emission. Another important dividing frequency is the so-called Schroeder frequency [22], defined as

$$f_s = 2000\sqrt{\frac{T_{60}}{V}}, \quad (4)$$

where the reverberation time is given by the Sabine equation [23] $T_{60} = 0.161V/S\alpha$, with $S$ being the total surface area of the room and $\alpha$ being the absorption coefficient, estimated by $\alpha = 1 - |(Z - Z_0)/(Z + Z_0)|^2$. Hence, for hard boundary $Z = 10^3 Z_0$, $f_s \cong 15f_0$. Schroeder frequency divides the results into the high-frequency regime ($f > f_s$), where the statistical-acoustics model is applicable, and the low-frequency regime ($f < f_s$), where the room behaves like an acoustic resonant cavity, with the interference effect playing an important role.

## III. IMPEDANCE OF RESONANCE-BASED METAMATERIALS

Constant and tunable surface impedance over a wide frequency range has been realized by resonance-based metamaterials [2,8]. A successful example that achieved $Z = Z_0$ for sound absorption, based on integrated Fabry-Perot resonators, can be found in Ref. [6]. In order to make the present work self-contained, below we give a brief recapitulation of the theoretical framework underlying this achievement.

Consider an idealized collection of resonances with a continuum distribution of resonance frequencies. Then the acoustic impedance takes the Lorentzian form [24]:

$$Z(\omega) = i\frac{Z_0 d}{\omega c_0}\left[\int_{\Omega_c}^{\infty} \frac{\alpha(\Omega)D(\Omega)}{\Omega^2 - \omega^2 - i\beta\omega}d\Omega\right]^{-1}, \quad (5)$$

where $Z_0$ is the impedance of air, $c_0$ is the sound speed in air, $d$ is the thickness of the sample material, and $\alpha_n, \Omega, \beta$
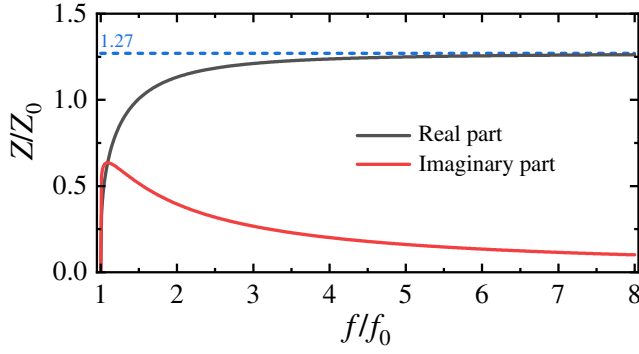
FIG. 2. Real and imaginary parts of impedance for idealized resonance-based metamaterials, designed for achieving $Z = \lambda Z_0$ above $f_0$. Here $\lambda = 1.27$.

denote the oscillation strength, angular resonance frequency, and dissipation coefficient, respectively. In addition, $\Omega_c = 2\pi f_c$ is the low-frequency cutoff and $D(\Omega)$ is the resonant-mode density defined by $D(\Omega) = dN/d\Omega$. Our target is to attain $Z = \lambda Z_0$ above $\Omega_c$. Due to the fact that dissipation of airborne sound is small (i.e., $\beta \ll \omega$), we can utilize the definition of Dirac delta function [25] to obtain

$$\frac{\rho_0 d}{Z(\omega)} = -i\omega P \int_{\Omega_c}^{\infty} \frac{\alpha(\Omega)D(\Omega)}{\Omega^2 - \omega^2} d\Omega$$
$$+ \pi\omega \int_{\Omega_c}^{\infty} \alpha(\Omega)D(\Omega)\delta\left(\Omega^2 - \omega^2\right) d\Omega. \quad (6)$$

The principal value of the first term is approximately zero, owing to its oscillatory nature. Hence Eq. (6) can be simplified as $\alpha(\omega)D(\omega) \cong 2d\rho_0/\pi Z(\omega)$. The target $Z = \lambda Z_0$ requires that

$$\alpha(\omega)D(\omega) = \frac{2\rho_0 d}{\lambda \pi Z_0}. \quad (7)$$

By substituting Eq. (7) into Eq. (5) and taking $\omega \to 2\pi f$, we have

$$Z(f) = i \lim_{\beta \to 0} \frac{Z_0 d}{\omega c_0} \left( \int_{\Omega_c}^{\infty} \frac{2d\rho_0/\lambda \pi Z_0}{\Omega^2 - \omega^2 - i\beta\omega} d\Omega \right)^{-1}$$
$$= \frac{\lambda Z_0}{1 - 2i \tanh^{-1}\left(f_c/f\right)/\pi}, \quad (8)$$

which has both real and imaginary parts as plotted in Fig. 2. The real part quickly approaches $Z_0$ above the cutoff frequency, whereas the imaginary part decays towards zero. In the following sections, we set $f_c$ slightly lower than the room's characteristic frequency $f_0$, to avoid the zero value of Re[$Z$]. The reason why Eq. (8) is not exactly the same as the target $Z = \lambda Z_0$ is that we adopt the approximation of neglecting the imaginary part of the impedance in

reducing Eq. (6) to Eq. (7). Also, the necessary existence of Im[$Z(\omega)$] can be explained by the Kramer-Kronig relation [26] and causality constraint [27] (i.e., it is impossible to create perfectly impedance-matched passive materials broadbandly with a finite thickness [6]).

In brief, this theoretical scheme provides a general design strategy for metamaterials with different forms of $\alpha(\omega)$. The required $D(\omega)$ value can be obtained from Eq. (7) according to the desired impedance; and the corresponding mode density may be realized by adjusting the geometry of the resonators.

## IV. NUMERICAL RESULTS FOR MINIMIZING GLOBAL $L_e$

### A. Relation between global $L_e$ and impedance

We show in Figs. 3(a) and 3(b) the numerical results (using COMSOL Multiphysics, a finite-element analysis and solver software) for the multisource case. It is seen that for selected frequencies above $f_0$, there is always a valley in $L_e$ that represents a 20- to 25-dB drop at the optimal value of the wall impedance. The curve at the characteristic frequency $f_0$ behaves differently because it is in the transition regime where the wavelength is close to the characteristic size of the room. For all $f > f_0$ the optimal impedance differs only slightly for different frequencies but clusters around $Z = Z_0$, since $Z = Z_0$ represents impedance matching and hence total absorption for normally incident
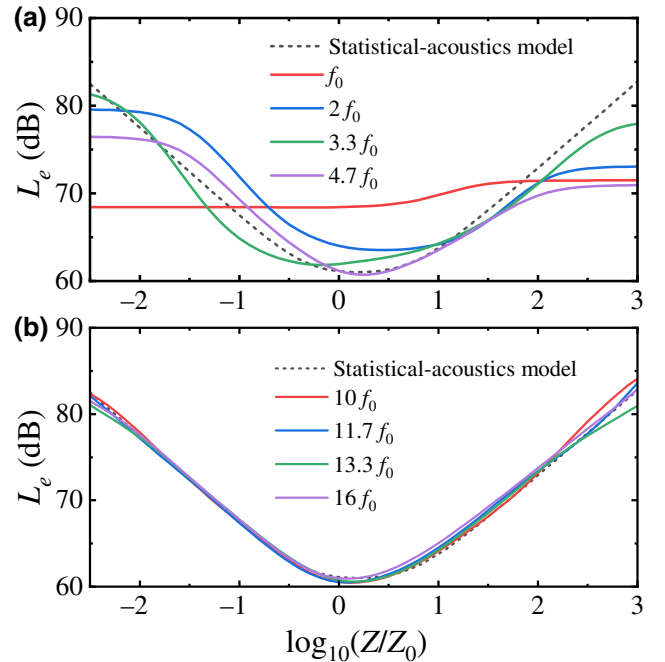


FIG. 3. (a) Relation between $L_e$ and surface impedance of the room (multisource case) for the low-frequency range. The dashed gray line denotes the results predicted by statistical-acoustics model. (b) The same relation for higher frequencies.
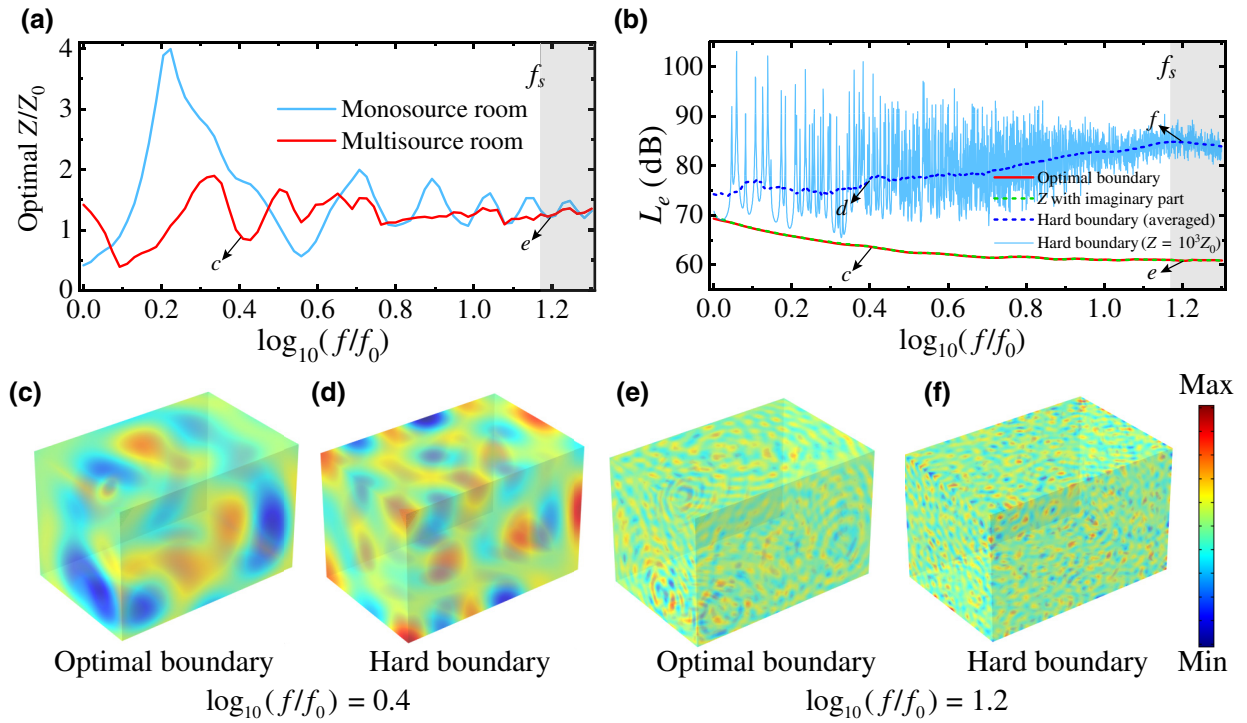
FIG. 4. (a) Optimal impedance plotted as a function of the logarithm of frequency for both the monosource (blue) and multisource cases (red). (b) Relation between global $L_e$ and $\log_{10}(f/f_0)$ for the two cases of the hard boundary and the optimal boundary. The blue dashed line is the averaged results (of the highly fluctuating blue line, reflecting the eigenfrequency effect of a hard wall cavity) with a moving window and the green dashed line represents the case with the impedance $Z(f)$ of real metamaterials, which have taken the imaginary part of the impedance into consideration. In both (a) and (b), the gray shaded region $f \geq f_s$ is the high-frequency regime where the statistical-acoustics model can work well. (c)–(f) Sound-pressure-field patterns for selected frequencies and surface boundaries, which correspond to the points $c, d, e, f$ marked in (a) and (b).

acoustic waves. The deviation from the exact $Z = Z_0$ condition is caused by the angular averaging of the incident waves, as most of the waves are not normally incident on the boundary (see detailed derivation in Appendix D). Further simulations also indicate that the positions and the number of the sound sources do not have a significant effect on the global $L_e$.

For frequencies close to or higher than $f_s$, results of analytical statistical-acoustics model (see detailed derivation in Appendix E) agree well with the numerical results, as illustrated in Fig. 3(b). Statistical-acoustics model treats waves as rays or particles and acoustic energy tends to spread isotropically. Since the sound rays are incoherent, their energy can be treated as the linear combination of two parts: one is the direct sound caused by spherical waves from sound sources, corresponding to the red line in Fig. 4(b); the other part is the reverberated sound due to the multiple reflection, which can be evaluated by the reduced $L_e$ [i.e., the gap between blue and red line in Fig. 4(b)]. However, for low frequencies [see Fig. 3(a)], statistical-acoustics model cannot be accurate owing to the fact that the effect of finite wavelength cannot be ignored, and interference plays an important role [see the sound-field patterns in Figs. 4(c)–4(f)]. It should be noted

that the amount of global $L_e$ reduction is independent of the noise source power, since the problem is in the linear acoustics regime.

### B. Relation between optimal impedance and frequency

The basic behavior of having a $L_e$ minimum is very robust for both monosource and multisource cases. Hence in Fig. 4(a), the optimal impedance is plotted in terms of its ratio to air impedance, as a function of normalized frequency. Comparison with the monosource case shows that the optimal impedance can oscillate as a function of frequency, and this oscillation weakens with increasing frequency and also with the increase in the number of sound sources. Such oscillations can be interpreted to originate from the interference effect that reflects the existence of acoustic eigenmodes (see Appendix C). With the frequency increasing to $f_s$, the mean value of the optimal impedance for both monosource and multisource cases approaches the value $Z = 1.27Z_0$.

### C. $L_e$ spectra with the optimal impedance and hard boundary

It is instructive to compare global $L_e$ for a room with hard boundary to that with the optimal impedance.
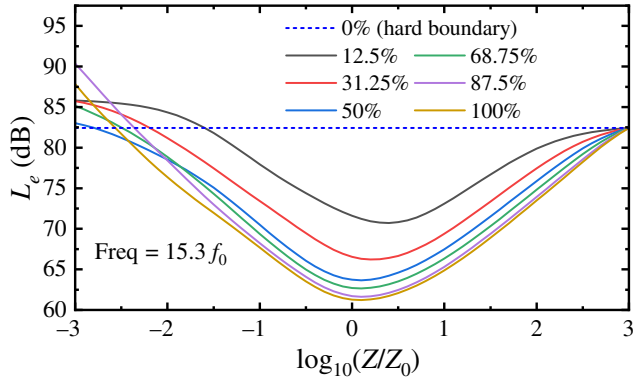
FIG. 5. Relation between $L_e$ and logarithm of impedance for varying coverage at $f = 15.3f_0$. The plotted results are representative of other frequencies as well.

Figure 4(b) shows that when averaged over all frequencies in the high-frequency regime, a room with optimal impedance can have a up to 15.5 dB lower $L_e$ (the averaged gap between the red and dashed blue curve) than that of a room with the hard boundary. It should be noted that we average $L_e$ with the hard boundary using a moving window. Since the room with the hard boundary acts like a cavity with a high quality factor below $f_s$, the oscillations of $L_e$ are caused by resonances. In fact, the frequencies of the sharp peaks [see blue line in Fig. 4(b)] coincide with the eigenfrequencies of the room (see Appendix C).

Also, in Fig. 4(b) the imaginary part of the impedance is taken into consideration (green dashed line), by replacing the constant surface impedance with that given by Eq. (8) ($\lambda = 1.27$ with the corresponding complex value). It is shown that the imaginary part of the impedance has negligible effects on global $L_e$, as seen from the fact that the green dashed line with $Z(f)$ almost coincides exactly with the red line that is calculated with the real-valued optimal impedance.

## D. Effectiveness of partial coverage of the room surfaces

How effective can the metamaterial be in reducing the global $L_e$ if only part of the room surfaces is covered by acoustic metamaterials with the rest being the hard boundary? The results that can answer this question are shown in Fig. 5. It is seen that even with 1/8 of the room surface covered by optimized acoustic metamaterials with the optimal impedance, there can already be more than 10-dB reduction in $L_e$. The optimal impedance, however, is shifted to a larger value than that for the 100% coverage. A 50% coverage can be almost as effective as total coverage, with only 5 dB less than total coverage. From the perspective of saving materials, only four walls (with 68.75% coverage) can already achieve over 95% of the global $L_e$ reduction effect.
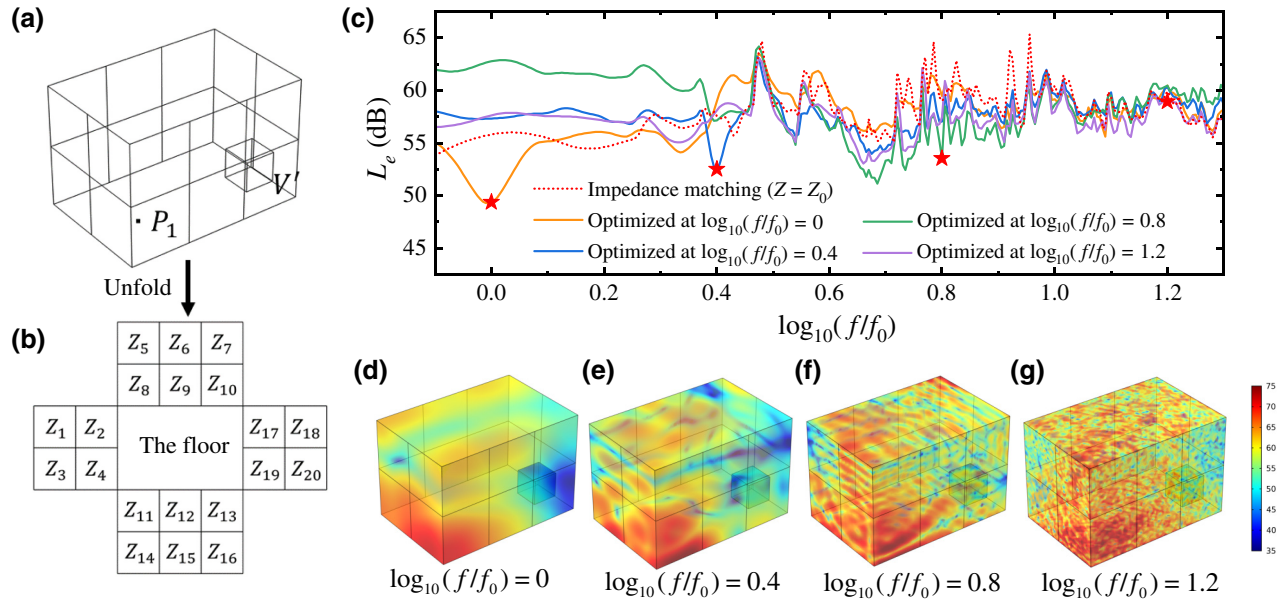


FIG. 6. (a) Schematics of an enclosed room for local $L_e$ reduction. $P_1$ is the sound source and $V'$ is the volume where the averaged local $L_e$ is evaluated. (b) A flat view of discretized wall areas, labeled with different impedance values. (c) Optimized local $L_e$ spectra for different targeted frequencies, marked as red stars. For comparison, the red dashed line denotes the noise spectrum of sound source (i.e., local $L_e$ caused by direct sound with impedance-matching condition). (d)–(g) Sound-pressure-field patterns for four optimized frequencies.

## V. NUMERICAL RESULTS FOR MINIMIZING LOCAL $L_e$

In this section, we aim at minimizing local $L_e$, i.e., averaged $L_e$ in a cubic volume $V'$ with the dimension of $0.5 \times 0.5 \times 0.5$ m$^3$ centered at (2.5 m, 0.5 m, 0.5 m) [see Fig. 6(a)]. For simplicity, only the source $P_1$ located at a corner is activated, which is treated as the noise source. Also, the ceiling and floor are treated as hard boundaries. The side-wall areas are discretized into 20 squares with equal size [see Figs. 6(a) and 6(b)]. Each square area is allocated with an impedance value $Z_i$ ($i = 1, 2, \ldots, 20$). Hence our problem can be formulated to be the minimization of the objective function

$$L_e(Z_1, Z_2, \ldots, Z_{20}) = 10 \log_{10} \left( \frac{1}{V'} \int_{V'} \frac{\epsilon}{\epsilon_0} dV' \right), \quad (9)$$

at targeted frequencies. Genetic algorithm (an evolutionary algorithm for multivariable optimization [13]) is adopted to handle this problem. Here the optimization toolbox of MATLAB is used. A natural question is whether the local $L_e$ can be lower than that caused by direct sound from the noise source (i.e., by applying impedance-matching boundary condition that can lead to negligible wave reflection). The answer to this question is "yes," as illustrated in Fig. 6(c), which shows that at optimized four frequencies (marked with red stars), the amount of reduced local $L_e$ are 6.46, 5.07, 5.47, and 0.98 dB respectively, as compared to using near-total absorption surface impedance value throughout all the walls. For simplicity, the range of each impedance wall is set to be $\log_{10}(Z_i/Z_0) \in [0, 1]$. Here the optimized results are listed in Table I.

The results are understandable from the interference perspective. In the low-frequency regime ($f < f_s$), the interference significantly causes spatial inhomogeneity of energy. By properly adjusting $\{Z_i\}$, the nodes and antinodes of the sound field can be utilized to create a quiet zone in the room [see Figs. 6(d)–6(g)]. For higher frequencies ($f > f_s$), the quiet-zone effect is limited, since the energy tends to spread uniformly.

TABLE I.    Optimization results given by genetic algorithm for local $L_e$ minimization. The data in the second column are in the unit of $Z_0$.

| Frequency | Dataset $\{Z_i\} = \{Z_1, Z_2, \ldots, Z_{20}\}$ |
|---|---|
| $f = f_0$ | [8.69, 8.19, 1.13, 2.29, 8.39, 1.50, 8.58, 1.55, 9.36, 1.43, 1.04, 1.08, 1.00, 6.87, 8.83, 5.02, 2.97, 1.08, 1.10, 1.18] |
| $f = 10^{0.4} f_0$ | [6.57, 9.61, 4.69, 1.12, 1.09, 3.11, 1.41, 1.12, 3.21, 1.13, 9.19, 1.08, 2.71, 1.17, 1.12, 1.45, 5.06, 8.43, 1.67, 9.46] |
| $f = 10^{0.8} f_0$ | [1.04, 7.53, 9.19, 1.02, 1.20, 1.30, 4.23, 1.15, 1.47, 2.08, 7.60, 6.37, 7.20, 2.04, 2.63, 7.16, 8.71, 9.71, 1.52, 7.43] |
| $f = 10^{1.2} f_0$ | [1.11, 1.05, 9.09, 1.30, 1.49, 1.77, 2.87, 5.05, 1.91, 1.49, 1.49, 2.07, 1.93, 7.13, 2.60, 1.00, 3.74, 2.91, 1.12, 1.42] |

## VI. CONCLUDING REMARKS

In conclusion, we confirm the feasibility of applying tunable metamaterials in reducing both global and local $L_e$ in an enclosed room. Metamaterials with the optimal impedance that is slightly greater than $Z_0$ can reduce global $L_e$ significantly and work well over a broad frequency range. This particular value can be used as an important reference for the future application of metamaterials in room acoustics. Also, partial coverage is shown to be fairly effective and can save the cost of metamaterials for practical applications. By harnessing the spatial energy inhomogeneity of low-frequency waves in a room, a local quiet zone can be created for targeted frequencies by optimizing discrete impedance values on different wall locations. This study serves as a bridge linking room acoustics with the latest developed capability of acoustic metamaterials and may inspire more promising applications in the future, e.g., the objective can be extended to improving auditory experiences, and the development of active metamaterial surfaces may further broaden the realm of room acoustics.

## APPENDIX A: DETAILS OF THE SOUND SOURCES

The simulation work is carried out with two types of setups: one with five randomly placed sound sources, denoted multisource, and another one with one source, denoted monosource. Information about sound sources are given in Table II. The position of the monosource is the same as the source no. 1 in the multisource case while its power is the summation of those of the multisource case.

## APPENDIX B: RELATION BETWEEN $L_e$ AND $L_p$

Level of sound energy intensity, adopted in this paper, can be related to sound-pressure level that is widely used

TABLE II.    Position, power, and phase of sound sources in a multisource room.

| Source no. | Location (m) | Power (W) | Phase |
|---|---|---|---|
| 1 | (0.4, 0.4, 0.4) | $3.43 \times 10^{-4}$ | 0 |
| 2 | (0.4, 0.8, 0.4) | $6.86 \times 10^{-4}$ | $\pi/3$ |
| 3 | (1.5, 1.0, 1.0) | $13.72 \times 10^{-4}$ | $\pi/6$ |
| 4 | (2.5, 0.5, 0.7) | $5.15 \times 10^{-4}$ | $\pi/4$ |
| 5 | (1.2, 1.8, 1.0) | $12.01 \times 10^{-4}$ | $\pi/8$ |

in acoustics. $L_e$ and $L_p$ [16] are, respectively, defined by

$$L_e = 10 \log_{10} \left( \frac{\epsilon}{\epsilon_0} \right), \qquad (B1)$$

$$L_p = 10 \log_{10} \left( \frac{p^2}{p_{\text{ref}}^2} \right), \qquad (B2)$$

where the reference energy intensity $\epsilon_0 = 10^{-12}$ W/m$^3$ and reference pressure $p_{\text{ref}} = 2 \times 10^{-5}$ Pa. But it should be noted that the conversion between $L_e$ and $L_p$ is valid only if the relevant wavelength is much smaller than the room size. With this condition, we can regard the sound propagation to comprise incoherent rays. Hence, sound energy intensity takes the form $\epsilon = I/c_0$ where the sound intensity $I = pv$. For sound rays, we regard the characteristic impedance $p/v$ of each ray as $Z_0$. From the above relations, we find the conversion relation between $L_e$ and $L_p$ given by

$$L_e - L_p = 10 \log_{10} \left( \frac{\epsilon}{\epsilon_0} \right) - 10 \log_{10} \left( \frac{p^2}{p_{\text{ref}}^2} \right)$$

$$= 10 \log_{10} \left( \frac{1}{Z_0 c_0} \frac{p_{\text{ref}}^2}{\epsilon_0} \right) \cong -25.5 \text{ dB}. \qquad (B3)$$

This relation is only applicable in the high-frequency regime where the statistical-acoustics model is accurate. In the lower frequencies, there can be significant interference effect and the impedance can no longer be treated as a constant $Z_0$, i.e., $L_p$ cannot be accurate any more.

## APPENDIX C: EIGENFREQUENCIES OF HARD AND SOFT BOUNDARY

In this section, we calculate the eigenfrequencies of rectangular room and then show that the frequency of the lowest nonzero eigenmode with soft boundary (SB) is necessarily higher than that of hard boundary (HB). The acoustic wave equation can be expressed in terms of the scalar Helmholtz equation for time harmonic waves:

$$\nabla^2 p - \frac{1}{c_0^2} \frac{\partial^2 p}{\partial t^2} = 0 \Rightarrow \nabla^2 p + |\mathbf{k}|^2 p = 0, \qquad (C1)$$

where the wavevector $\mathbf{k} = (k_x, k_y, k_z)$ and $|\mathbf{k}| = \omega/c_0$. The eigenmodes can be obtained by solving Eq. (C1) with proper boundary conditions, which are specified as $\mathbf{n} \cdot \nabla p = 0$ for the hard boundary and $p = 0$ for the soft boundary. Here $\mathbf{n}$ is the unit vector normal to the boundary. For a room with the dimension of $l_x \times l_y \times l_z$, the eigenmodes [16] with hard-boundary condition can be expressed

TABLE III. List of the lowest ten eigenfrequencies. The symbols $\sqrt{}$, $\times$ represent the existence and nonexistence of nonzero eigenmodes, respectively.

| No. | Eigenfrequency | Relevant mode | HB | SB |
|-----|----------------|---------------|-----|-----|
| 1 | $0.381 f_0$ | $(1, 0, 0)$ | $\sqrt{}$ | $\times$ |
| 2 | $0.572 f_0$ | $(0, 1, 0)/(0, 0, 1)$ | $\sqrt{}$ | $\times$ |
| 3 | $0.687 f_0$ | $(1, 0, 0)/(1, 0, 1)$ | $\sqrt{}$ | $\times$ |
| 4 | $0.762 f_0$ | $(2, 0, 0)$ | $\sqrt{}$ | $\times$ |
| 5 | $0.809 f_0$ | $(0, 1, 1)$ | $\sqrt{}$ | $\times$ |
| 6 | $0.894 f_0$ | $(1, 1, 1)$ | $\sqrt{}$ | $\sqrt{}$ |
| 7 | $0.953 f_0$ | $(2, 1, 0)/(2, 0, 1)$ | $\sqrt{}$ | $\times$ |
| 8 | $1.112 f_0$ | $(2, 1, 1)$ | $\sqrt{}$ | $\sqrt{}$ |
| 9 | $1.143 f_0$ | $(3, 0, 0)/(0, 2, 0)/(0, 0, 2)$ | $\sqrt{}$ | $\times$ |
| 10 | $1.206 f_0$ | $(1, 2, 0)/(1, 0, 2)$ | $\sqrt{}$ | $\times$ |

as

$$p = p_0 \cos(k_x x) \cos(k_y y) \cos(k_z z)$$

$$= p_0 \cos \left( \frac{n_x \pi}{l_x} x \right) \cos \left( \frac{n_x \pi}{l_y} y \right) \cos \left( \frac{n_z \pi}{l_z} z \right), \quad (C2)$$

where $(n_x, n_y, n_z)$ are integers. Similarly, the eigenmodes with soft-boundary condition are

$$p = p_0 \sin(k_x x) \sin(k_y y) \sin(k_z z)$$

$$= p_0 \sin \left( \frac{n_x \pi}{l_x} x \right) \sin \left( \frac{n_x \pi}{l_y} y \right) \sin \left( \frac{n_z \pi}{l_z} z \right). \quad (C3)$$

Hence the eigenfrequency for the mode $(n_x, n_y, n_z)$ is

$$f_{n_x, n_y, n_z} = \frac{c_0}{2} \sqrt{ \left( \frac{n_x}{l_x} \right)^2 + \left( \frac{n_y}{l_y} \right)^2 + \left( \frac{n_z}{l_z} \right)^2 }. \qquad (C4)$$

According to Eq. (C4), the lowest ten eigenfrequencies are listed in Table III, for the room with the dimensions $l_x = 3$ m, $l_y = 2$ m, $l_z = 2$ m. We can see that the lowest mode for hard boundary is $(1, 0, 0)$. However, for soft boundary, the lowest mode is $(1, 1, 1)$, where $(n_x, n_y, n_z)$ cannot be zero components. Because $f_{111} > f_{100}$, we conclude that the lowest eigenfrequency for soft boundary is higher than that of hard boundary. Because modes with zero component(s) degenerate to zero mode when applying soft boundary, the mode density of soft boundary is always lower than that of hard boundary for a rectangular room. So far the energy loss and absorption of the room has not been taken into consideration. Thanks to the numerical eigenmode solver of COMSOL Multiphysics, the eigenfrequencies can be plotted as a function of normalized frequencies (see Fig. 7). In this way, the loss can be reflected by the imaginary part of eigenfrequencies. It is interesting that some eigenmodes disappear (i.e., degenerate to zero mode) near the transition region $Z \to Z_0$. The results in Fig. 7 are consistent with that of Table III. Below $f_0$, there is only one eigenmode for
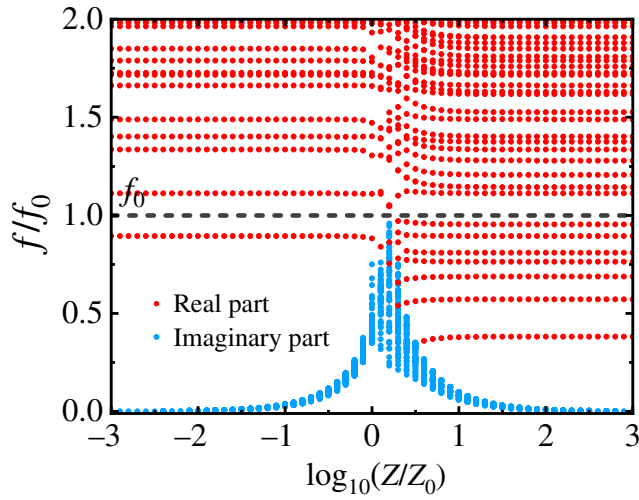
FIG. 7. Real and imaginary parts of the eigenfrequencies, plotted as a function of normalized impedance.

soft boundary, i.e., energy emission of sound source can be significantly suppressed.

## APPENDIX D: ANGLE-AVERAGED ABSORPTION COEFFICIENT

Consider the form of the absorption coefficient for single incident angle $\theta$:

$$
\begin{aligned}
\alpha_\theta &= 1 - |r_p|^2, \\
&= 1 - \left| \frac{Z\cos\theta - Z_0}{Z\cos\theta + Z_0} \right|^2, \\
&= \frac{4 x_n \cos\theta}{(x_n \cos\theta + 1)^2},
\end{aligned} \tag{D1}
$$

where normalized impedance is defined by $Z/Z_0 = x_n$. Angle-averaged absorption coefficient [21] is defined as the ratio between the absorbed energy for all angles and the total incident energy for all angles:

$$
\alpha = \frac{\Delta E_a}{\Delta E}. \tag{D2}
$$

We assume that the average energy density in the room is $\bar{\epsilon}$. Now we express the $\Delta E$ by integrating over the solid angle and volume:

$$
\begin{aligned}
\Delta E &= \int d(\Delta E) = \int \bar{\epsilon}\, dV \frac{d\Omega}{4\pi}, \\
&= \int_0^{\pi/2} \bar{\epsilon}(2\pi r^2 \sin\theta\, d\theta\, dr) \frac{dS}{4\pi r^2}, \\
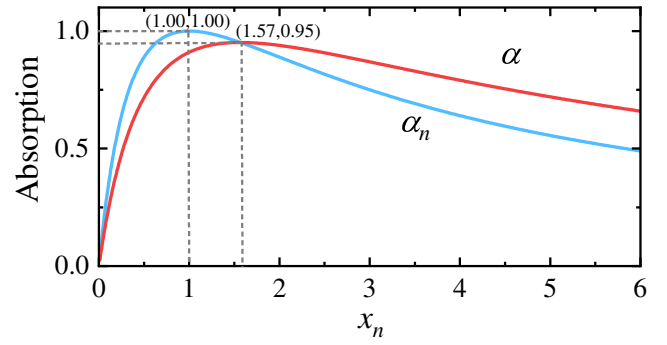&\cong \frac{\bar{\epsilon}}{4} \Delta S \Delta r.
\end{aligned} \tag{D3}
$$



FIG. 8. Normal incidence absorption $\alpha_n$ and angel-averaged absorption $\alpha$ plotted as a function of normal impedance $x_n$. Here $\alpha_n = 1 - |(x_n - 1)/(x_n + 1)|^2$ and $\alpha$ is given by Eq. (D5).

$\Delta E_a$ can be calculated in the similar way:

$$
\begin{aligned}
\Delta E_a &= \int d(\Delta E_a) = \int \alpha_\theta \bar{\epsilon}\, dV \frac{d\Omega}{4\pi}, \\
&= \int_0^{\pi/2} \alpha_\theta \bar{\epsilon}(2\pi r^2 \sin\theta\, d\theta\, dr) \frac{dS}{4\pi r^2}, \\
&\cong \frac{\bar{\epsilon}}{2} \Delta S \Delta r \int_0^{\pi/2} \alpha_\theta \cos\theta \sin\theta\, d\theta.
\end{aligned} \tag{D4}
$$

By inserting $\Delta E$ and $\Delta E_a$ into Eq. (D2), we obtain angle-averaged absorption by integrating over $\theta$:

$$
\begin{aligned}
\alpha &= \frac{\Delta E_a}{\Delta E} = \int_0^{\pi/2} 2\alpha_\theta \cos\theta \sin\theta\, d\theta, \\
&= \frac{8}{x_n^2}\left[ 1 + x_n - \frac{1}{1+x_n} - 2\ln(1+x_n) \right].
\end{aligned} \tag{D5}
$$

Hence, the optimal impedance must deviate from $Z_0$, as shown in Fig. 8. In particular, two limits of Eq. (D5) are

$$
\lim_{x_n \to 0} \alpha = \frac{8 x_n}{3}, \tag{D6}
$$

$$
\lim_{x_n \to \infty} \alpha = \frac{8}{x_n}. \tag{D7}
$$

## APPENDIX E: THEORY OF THE STATISTICAL-ACOUSTICS MODEL

In this section, an analytical relation between $L_e$ and surface impedance is derived based on the classical statistical-acoustics model. To begin with, the total energy density of an enclosed room at a specific location **r** is divided into two parts:

$$
\epsilon(\mathbf{r}) = \epsilon_D + \epsilon_R, \tag{E1}
$$

where $\epsilon_D$ and $\epsilon_R$ represent sound intensity of direct sound and reverberated sound, respectively. Equation (E1) is

applicable in the high-frequency regime, where the sound waves can be treated as particles and incoherent rays. Explicit expressions of $\epsilon_D$ and $\epsilon_R$ can be obtained from energy conservation.

On one hand, since a sound source has a spherical wavefront, its sound intensity **I** (i.e., energy flux), defined by $c_0 \epsilon_D \mathbf{e}_r$, satisfies that

$$\int_S \mathbf{I} d\mathbf{S} = \int_S c_0 \epsilon_D d(4\pi r^2) = W_i, \qquad \text{(E2)}$$

where $W_i$ is the power of the source and $S$ is a spherical surface that contains the source. So $\epsilon_D$ with a distance $r$ to the sound source is $\epsilon_D = W_i/4\pi c_0 r^2$. Considering the multisource case, it can be revised as

$$\epsilon_D = \sum_{i=1}^{5} \frac{W_i}{4\pi c_0 (\mathbf{r} - \mathbf{r}_i)^2}, \qquad \text{(E3)}$$

where $\mathbf{r}_i = (x_i, y_i, z_i)$ is the location of one of the sound sources, as displayed in Table II.

On the other hand, the direct sound rays are reflected by the surfaces and reverberated to form a flat energy distribution, after long enough time, i.e., only the steady-state case is considered. The mean free path [16] of sound rays is given by $\bar{l} = 4V/S$, i.e., mean distance of two reflections. Here $V$ and $S$ are volume and surface area of the room, respectively. Hence, the sound ray will reflect $c_0 S/4V$ times per second. The absorbed reverberated sound energy per second is $\alpha(\epsilon_R V)(c_0 S/4V)$. It should be noted that $\epsilon_R$ is not a function of spatial coordinates. The energy offered by sound sources per second is $W(1 - \alpha)$, where the total power $W = \sum W_i$. Energy conservation relation should be

$$\alpha(\epsilon_R V)\frac{c_0 S}{4V} = W(1 - \alpha). \qquad \text{(E4)}$$

So the reverberated energy density is given by

$$\epsilon_R = \frac{4W}{Rc_0}, \qquad \text{(E5)}$$

where $R = S\alpha/(1 - \alpha)$ is the room constant [16]. By inserting Eq. (E1) into Eq. (2), we obtain

$$L_e = 10 \log_{10} \left[ \int_V \sum_i \frac{W_i}{(\mathbf{r} - \mathbf{r}_i)^2} \frac{dV}{4\pi \epsilon_0 c_0 V} + \frac{4W}{\epsilon_0 c_0 R} \right]. \qquad \text{(E6)}$$

According to Eqs. (D6) and (D7), if $x_n \to \infty$ (or $x_n \to 0$), we have $\alpha \to 0$ and thus $R \to 0$. Then the direct sound term of Eq. (E6) inside the square bracket can be ignored.

Also, room constant $\lim_{\alpha \to 0} R = 1/S\alpha$. By taking the logarithm of $x_n$ and denoting it as $y_n$, we can express $x_n = 10^{y_n}$. Hence, when $x_n \to \infty$, we obtain

$$L_e = 10 \log_{10} \left[ \frac{4W}{\epsilon_0 c_0 S} \frac{x_n}{8} \right],$$
$$= 10 \log_{10} \left[ \frac{W}{2\epsilon_0 c_0 S} \right] + 10 y_n. \qquad \text{(E7)}$$

Similarly, when $x_n \to 0$, we have

$$L_e = 10 \log_{10} \left[ \frac{4W}{\epsilon_0 c_0 S} \frac{3}{8x_n} \right],$$
$$= 10 \log_{10} \left[ \frac{3W}{2\epsilon_0 c_0 S} \right] - 10 y_n. \qquad \text{(E8)}$$

Equations (E7) and (E8) are exactly the two asymptotic limits of Eq. (E6), which is consistent with the fact that the left and right sides of the $L_e$ curve are linear, as shown in Figs. 3(a) and 3(b).

---

[1] Ping Sheng, *Introduction to Wave Scattering, Localization and Mesoscopic Phenomena*, (Springer Science & Business Media, New York, 2006), Vol. 88.

[2] Min Yang and Ping Sheng, Sound absorption structures: From porous media to acoustic metamaterials, Ann. Rev. Mater. Res. **47**, 83 (2017).

[3] Eberhard Zwicker and Hugo Fastl, *Psychoacoustics: Facts and Models* (Springer Science & Business Media, New York, 2013), Vol. 22.

[4] Jose Cucharero, Tuomas Hänninen, and Tapio Lokki, in *Acoustics* (Multidisciplinary Digital Publishing Institute, 2019), Vol. 1, p. 644.

[5] Mike Barron and L-J. Lee, Energy relations in concert auditoriums. I, J. Acoust. Soc. Am. **84**, 618 (1988).

[6] Min Yang, Shuyu Chen, Caixing Fu, and Ping Sheng, Optimal sound-absorbing structures, Mater. Horiz. **4**, 673 (2017).

[7] Steven A. Cummer, Johan Christensen, and Andrea Alù, Controlling sound with acoustic metamaterials, Nat. Rev. Mater. **1**, 16001 (2016).

[8] Guancong Ma and Ping Sheng, Acoustic metamaterials: From local resonances to broad horizons, Sci. Adv. **2**, e1501595 (2016).

[9] X. Sagartzazu, L. Hervella-Nieto, and J. M. Pagalday, Review in sound absorbing materials, Arch. Comput. Method E. **15**, 311 (2008).

[10] John W. Parkins, Scott D. Sommerfeldt, and Jiri Tichy, Narrowband and broadband active control in an enclosure using the acoustic energy density, J. Acoust. Soc. Am. **108**, 192 (2000).

[11] A. J. Bullmore, P. A. Nelson, A. R. D. Curtis, and S. J. Elliott, The active minimization of harmonic enclosed sound fields, part ii: A computer simulation, J. Sound Vib. **117**, 15 (1987).

[12] S. K. Lau and S. K. Tang, Sound fields in a rectangular enclosure under active sound transmission control, J. Acoust. Soc. Am. **110**, 925 (2001).

[13] Darrell Whitley, A genetic algorithm tutorial, Stat. Comput. **4**, 65 (1994).

[14] Guancong Ma, Xiying Fan, Ping Sheng, and Mathias Fink, Shaping reverberating sound fields with an actively tunable metasurface, Proc. Natl. Acad. Sci. **115**, 6638 (2018).

[15] Ivo Micha Vellekoop and A. P. Mosk, Phase control algorithms for focusing light through turbid media, Opt. Commun. **281**, 3071 (2008).

[16] Heinrich Kuttruff, *Room Acoustics* (CRC Press, Boca Raton, 2016).

[17] Finn Jacobsen and Alfonso Rodríguez Molares, Statistical properties of kinetic and total energy densities in reverberant spaces, J. Acoust. Soc. Am. **127**, 2332 (2010).

[18] Yun Jing and Ning Xiang, A modified diffusion equation for room-acoustic predication, J. Acoust. Soc. Am. **121**, 3284 (2007).

[19] Lauri Savioja and U. Peter Svensson, Overview of geometrical room acoustic modeling techniques, J. Acoust. Soc. Am. **138**, 708 (2015).

[20] Barry Parker, *Good Vibrations: The Physics of Music* (JHU Press, Baltimore, 2009).

[21] Philip McCord Morse and K. Uno Ingard, *Theoretical Acoustics* (Princeton university press, Princeton, 1986).

[22] Manfred R. Schroeder, Statistical parameters of the frequency response curves of large rooms, J. Audio Eng. Soc. **35**, 299 (1987).

[23] W. C. Sabine, *Collected Papers on Acoustics* (University Press Harvard Reprinted by Dover, New York (1964), 1922).

[24] Min Yang and Ping Sheng, An integration strategy for acoustic metamaterials to achieve absorption by design, Appl. Sci. **8**, 1247 (2018).

[25] Michael Stone and Paul Goldbart, *Mathematics for Physics: a Guided Tour for Graduate Students* (Cambridge University Press, Cambridge, 2009).

[26] John David Jackson, *Classical Electrodynamics* (John Wiley & Sons, Hoboken, 2007).

[27] Konstantin N. Rozanov, Ultimate thickness to bandwidth ratio of radar absorbers, IEEE T. Antenn. Propag. **48**, 1230 (2000).